

An Extended Adaptive Subspace Self-Organizing Map (EASSOM) Imbalanced Learning and Its Applications in EEG

Zehong Cao, *Member IEEE*, Yu-Ting Liu, Chun-Hsiang Chuang, *Member IEEE*, Yang-Yin Lin, Tsung-Yu Hsieh, Chieh-Ning Fang, Nikhil R. Pal, *Fellow IEEE*, and Chin-Teng Lin, *Fellow IEEE* *

Abstract—This paper presents a novel oversampling technique addressing highly imbalanced distributions in benchmark and electroencephalogram (EEG) datasets. Presently, conventional machine learning technologies do not adequately address imbalanced data with an anomalous class distribution and underrepresented data. To balance the class distributions, an extended adaptive subspace self-organizing map (EASSOM) that combines a local mapping scheme and the globally competitive rule is proposed to artificially generate synthetic samples that focus on minority class samples and its application in EEG. The EASSOM is configured with feature-invariant characteristics, including translation, scaling, and rotation, and it retains the independence of the basis vectors in each module. Specifically, basis vectors that are generated via each EASSOM module can avoid generating repeated representative features that only increase the computational load. Several benchmark experimental results demonstrate that the proposed EASSOM method incorporating a supervised learning approach could be superior to other existing oversampling techniques, and three EEG applications present the improvement of classification accuracy using the proposed EASSOM method.

Index Terms— Imbalanced Learning, Oversampling, Synthetic Sample Generation, Subspace, EEG, Classification

I. INTRODUCTION

LEARNING from imbalanced data has attracted growing attention in the research community in recent years because it is present in a variety of real-world application problems, including medical diagnosis, anomaly detection, and financial fraud detection [1-4]. Under these circumstances, the use of computationally intelligent methods has the potential to play an essential role in solving these problems; however, there are still many challenges to this research topic.

Specifically, a classification task can be regarded as an imbalanced problem whenever some types of data distribution

significantly dominate the others. In this paper, for simplicity, we focus on the two-class imbalanced classification problem, which is a topic of major interest in the research community. The underlying challenge manifests itself in two common forms: relative imbalance and absolute imbalance. Relative imbalance occurs when minority samples are well represented but severely outnumbered by the majority of samples, whereas absolute imbalance arises in datasets in which minority samples are scarce and underrepresented. Either form of imbalance poses a great challenge to conventional classification algorithms because it becomes extremely difficult to detect minority class samples. The reason arises from the fact that the algorithm tends to favor the majority class samples or simply omit the minority class samples in the training process, which thereby results in a biased classifier. This phenomenon becomes troublesome when the detection of minority class samples is crucially important, such as in cancer diagnosis.

Current solutions to the imbalanced problem can be divided into two categories: internal methods and external methods. Internal methods target the imbalanced problem by modifying the underlying classification algorithm. A popular approach in this category is cost-sensitive learning [5], which uses a cost matrix for different types of errors or instances to facilitate the learning directly from an imbalanced dataset. A higher cost of misclassifying a minority class sample compensates for the scarcity of the minority class. In [6], a cost-sensitive framework for applying the support vector machine is proposed. In [7], Zhou and Liu investigated the applicability of cost-sensitive neural networks on the imbalanced classification problem. In contrast, external methods aim to address the imbalanced problem by manipulating the input data to form a more balanced data set. External methods can further be divided into under-sampling and oversampling. Under-sampling methods compensate for the imbalanced problem by reducing the instances of the majority class. A cluster-based under-sampling approach is proposed in [8]. A study demonstrates class cover catch diagrams (CCCDs) capture the density of majority class as radii of the covering balls as to preserve the information during the under-sampling process [9]. In contrast to under-sampling methods that remove majority class samples, oversampling methods balance the data set by generating synthetic samples for the minority classes. The synthetic minority oversampling technique (SMOTE) [10] algorithm generates an arbitrary number of synthetic minority samples to eliminate the classifier learning bias. A collection of extension works based on the SMOTE algorithm has been proposed to address the imbalanced classification problem, e.g., the Borderline-SMOTE [11], SMOTE-Boost [12], majority weighted minority oversampling technique (MWMOTE) [13] and adaptive synthetic sampling (ADASYN) [14]. In [15], an

This work was supported by the Australian Research Council (ARC) [DP180100670, DP180100656]. The research was also sponsored in part by the Army Research Laboratory and was accomplished under Cooperative Agreement Numbers W911NF-10-2-0022 and W911NF-10-D-0002/TO 0023. (*Corresponding Author: C.T. Lin)

Z. Cao is affiliated with the Discipline of ICT, University of Tasmania, and School of Computer Science, University of Technology Sydney, Australia.

C.T. Lin, Y.T. Liu, C.H. Chuang, C.N. Fang are affiliated with the Center for Artificial Intelligence and Faculty of Engineering and Information Technology, University of Technology Sydney, Australia.

N. R. Pal is with the Institute of Electrical Control Engineering, Indian Statistical Institute, India.

Y.Y. Lin is with the Brain Research Center, National Chiao Tung University, Taiwan.

T.Y. Hsieh is with College of Information Sciences and Technology, University of Pennsylvania, Philadelphia, USA.

enhanced structure-preserving oversampling (ESPO) method that is based on a combination of the multivariate Gaussian distribution and an interpolation-based algorithm is developed. In [16], we proposed a kernel adaptive subspace method to address nonlinear boundary problems. Kernel method achieves remarkable performance on extremely imbalanced data but comes with a high computational cost.

Inspired by the adaptive subspace self-organizing map (ASSOM) proposed by T. Kohonen in [17] and [18], it consists of different modules where each module learns to recognize invariant patterns that are subjected to simple transformation (each module represents a subspace). Thus, each subspace represents some invariant characteristics of a subset of the data. It is, therefore, reasonable to assume that if we can generate synthetic instances from each of these subspaces, these instances will follow the distribution of the original data. We shall exploit this property to deal with classification with imbalanced data. Thus, in this paper, we proposed an extended adaptive subspace self-organizing map (EASSOM)-based oversampling method to address the imbalanced problem.

Considering that the patterns of neurons may represent the patterns of brain dynamics, the proposed method may be applied in imbalanced-based brain-computer interfaces. For example, in terms of electroencephalogram (EEG) applications, motor imagery (MI) signals recorded via electroencephalography (EEG), a mental process by which an individual rehearses or simulates a given action, is the most convenient basis for designing brain-computer interfaces [19, 20]. This helps motor disabled people to communicate with the device by performing a sequence of MI tasks, but the motor imagery samples were usually found highly imbalanced. Furthermore, clinical applications of EEG have increasingly gained attention within the biomedical engineering community. It can be applied to end-users with prediction or classification of neurological diseases, including migraine [21], depression [22], and sleep [23]. However, the minority of EEG samples may lead to a negative influence on classification accuracy. This study tries to tackle the same problem with merely linear computation involved. The EASSOM is feature-invariant regarding translation, scaling, and rotation. By assuring the independence of the basis vectors of each module, we can generate representative synthetic EEG samples for the minority class.

The remainder of this paper is organized as follows. In Section 2, a concise survey of existing oversampling techniques is presented. The details of the proposed EASSOM algorithm are discussed in Section 3. Section 4 discusses the experimental results on various benchmark data and provides a comparison with other existing oversampling algorithms. Section 5 presents the experimental results on EEG data collected in this study. Finally, conclusions are drawn in Section 6.

II. RELATED WORK

The critical issue in imbalanced data is that learning algorithms tend to be biased toward majority classes or less important negative classes that consist of a large number of samples. Methods to overcome imbalances can be divided into two main categories [24] [25]. The first category is a data-level method that runs on the training set and changes its class

distribution, designed to change the data set to make standard training algorithms work properly, such as over-sampling and under-sampling technologies. Another category covers classifier-level methods that keep the training data set unchanged and adjust the training or inference algorithm, including thresholding (adjusting the decision threshold of the classifier for neural network estimation of Bayesian posterior probability) and cost-sensitive learning (assigning different costs of misclassifying examples from different categories) [26] [27].

In this study, we will focus on the first category-oversampling technology. For a two-class imbalanced problem, various oversampling approaches have been proposed to balance the distribution of different classes, including SMOTE [10], ADASYN [14], ESPO [15], MWMOTE [13] and ADG [28]. These methods alter the imbalanced ratios by augmenting the minority class (or positive class) with synthetically generated samples. Then, a classifier is trained according to the balanced dataset. This mechanism of oversampling has proven to improve the performance in the recognition task efficiently.

A. Synthetic Minority Over-sampling Technique

SMOTE [10] utilizes minority (positive) samples as seed samples and evenly generates synthetic samples from each selected seed. The minority class is oversampled by introducing synthetic samples along with the k -nearest neighbor (KNN) of the minority class. Synthetic samples are generated using the following steps: 1) taking the difference between a sample under consideration and its nearest neighbor, 2) multiplying this difference by a random number between 0 and 1, and 3) adding this weighted difference to the sample under consideration. This process causes the selection of a random point along with the line segment between two specific samples and effectively determines the decision boundary of the minority class, which causes the classifier to become more general in a classification task. In addition, in [10], the authors indicate that a combination of under-sampling the majority class and oversampling the minority class can provide superior system performance compared with either an under-sampling or an oversampling approach. The SMOTE that combines under-sampling of the majority class introduces a bias toward the minority class. Therefore, SMOTE provides more related minority class samples that a classifier can learn from, and the broader areas can be carefully carved, which results in a better approximation of the minority class. However, over-generalization in the SMOTE severely influences the system performance. The over-generalization in the SMOTE algorithm is mainly caused by its generated synthetic samples. Specifically, SMOTE gives the same number of synthetic data samples for each primitive minority sample and does not carefully consider the distribution of the neighboring samples, which leads to the occurrence of overlap between different classes.

B. Adaptive Synthetic Sampling

Various adaptive oversampling techniques have been proposed in the recent past to overcome the limitation of the SMOTE. The ADASYN [14] algorithm employs an adaptive mechanism in which the number of synthetic samples generated by each minority (positive) seed is determined by the ratio of

majority (negative) samples in its neighborhood. The nucleus of ADASYN is to evaluate the level of learning difficulty for each minority class sample. A weighted distribution approach is used to allocate specific weights to different minority samples, where more synthetic data would be generated for a minority sample that is more difficult to learn compared with minority samples that are easier to learn. As a result, the ADASYN approach improves the distribution of different classes in two phases, including 1) reducing the bias introduced by the class imbalance, and 2) adaptively adjusting the decision boundary with respect to the difficult regions. These two objectives are accomplished by a dynamic adjustment of the weights and an adaptive learning procedure according to the density distribution.

C. Enhanced Structure-Preserving Oversampling

ESPO [15] was proposed by Cao *et al.* to handle highly imbalanced time series classification. ESPO uses a multivariate Gaussian distribution to estimate the covariance matrix of the minority samples and regularize the unreliable *Eigen* spectrum. The central portion of synthetic samples is generated by ESPO in the *Eigen* decomposed subspace and is regularized by the *Eigen* spectrum. To aim to protect the seed samples that are difficult to classify in the minority class, an interpolation-based technique is employed to augment a smaller portion of the synthetic population. By preserving the main covariance architecture and creating protective variances in the trivial *Eigen* dimensions, the ESPO can successively generate synthetic samples that still have partial dissimilarity with respect to the existing minority class samples.

D. Majority Weighted Minority Oversampling Technique

Barua *et al.* proposed the MWMOTE [13], which identifies the most informative minority class samples that are more difficult to classify. To address this issue, the clustering approach is applied to adaptively assign appropriate weights to each of the minority samples according to their importance in the learning procedure. The samples that are closer to the decision boundary are given higher weights than others. Similarly, the samples of the small-sized clusters are given higher weights to reduce the within-class imbalance. As a result, the MWMOTE generates synthetic samples using those weighted seed samples. This architecture of the MWMOTE guarantees that each generated sample resides inside a certain minority class cluster, which prevents noisy synthetic sample generation. The MWMOTE is the first attempt at identifying the difficult-to-learn minority class samples and assigns them proper weights according to their Euclidian distance from the nearest majority class sample. The essence of the MWMOTE include 1) selecting the most informative subset from the primitive minority samples, 2) calculating the weights to the selected samples according to their importance (Euclidian distance) in the dataset, and 3) exploiting a clustering approach to augment the synthetic minority class samples.

E. Absent Data Generator

Pourhabib *et al.* proposed the ADG [28] to tackle the imbalanced problem by oversampling minority class. ADG employs kernel Fisher discriminant analysis to generate synthetic data near the discriminative boundary of minority, and

majority class as data close to boundary carry more information for hyperplane separation in the feature space.

F. Support Vector Machines for Class Imbalance

Support vector machines (SVMs) are a popular machine learning technique, which works effectively with balanced datasets. However, when it comes to imbalanced datasets, SVMs produce suboptimal classification models. *Joachims* proposed a support vector method, called SVM-light [29], for optimizing multivariate based on the sparse approximation algorithm for the structural SVM. Instead of learning a univariate rule that predicts the label of a single example, the SVM-light exploited a multivariate prediction of all examples in the dataset during the learning phase. The SVM-light can effectively address a large imbalance between positive and negative examples by directly optimizing the measure of interest (e.g., recall, precision, F-value). In addition, the “balanced” mode of SVM is also applied in this study to separate the hyperplane for imbalanced classes [30]. The “balanced” mode automatically adjusts weights inversely proportional to class frequencies in the input data.

III. THE EXTENDED ADAPTIVE-SUBSPACE SELF-ORGANIZING MAP (EASSOM)

The idea of using subspaces that are subsets of the largest principal components for data generation is an emerging technology. Our proposed EASSOM is handled by projecting existing minority instances onto these adaptive subspaces to generate synthetic instances. Our imbalance learning obtained synthetic instances can retain the characteristics of existing instances and may improve the learning efficiency and avoid overfitting of the training classifier. Then, an inverse transform is able to map the synthesized data in the feature space back to the original input space.

Here, we briefly elaborate on the generation of synthetic instances for imbalance learning. The network parameters are firstly initialized according to the target task. Then, the input instance is mapped to the feature space and projected onto different subspaces of the feature space. Furthermore, a weighted vector of each subspace is trained using a competitive learning scheme. What is more, the Gram-Schmidt process is applied in the feature space to generate an orthogonal basis. The training epochs will continue until a predetermined termination criterion is reached. Finally, a synthetic instance is generated by

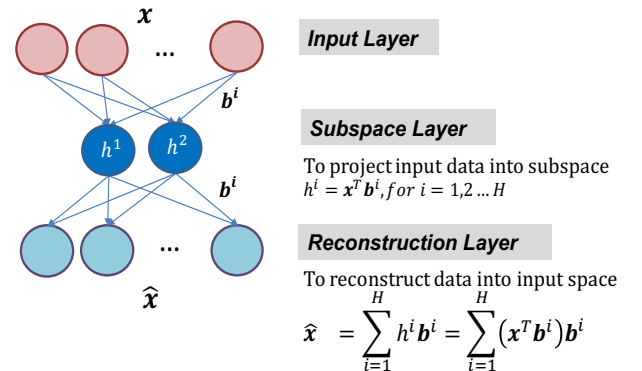


Figure 1. The architecture of the **EASSOM**

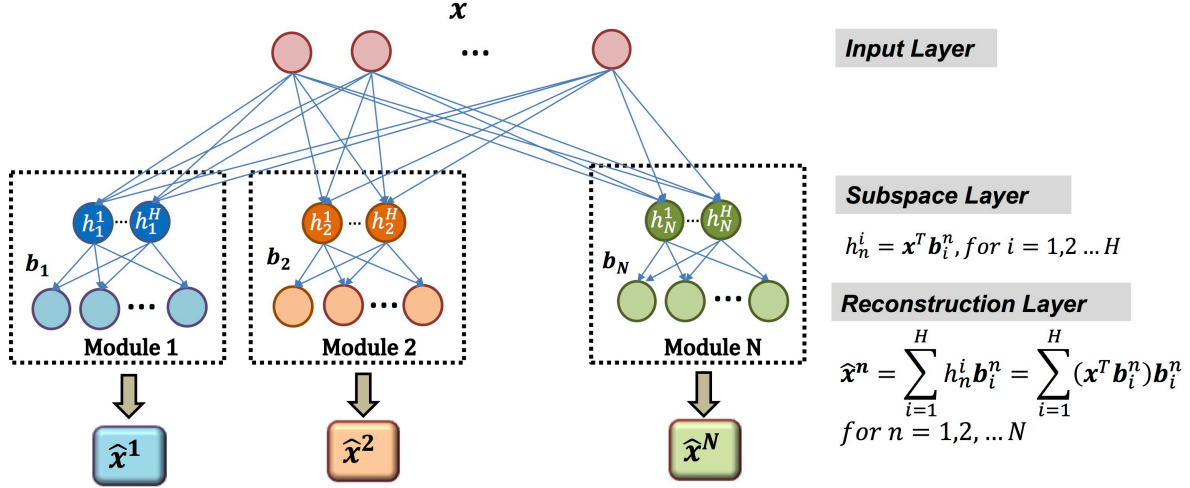


Figure 2. Competitive learning of EASSOM

projecting an existing instance onto a trained feature subspace and then inversely transforming the synthetic instance back to the input space. Therefore, each training instance can be used to generate as many synthetic instances as there are subspaces.

As shown in Figure 1, the proposed EASSOM model, which is extended by the concept of ASSOM, a special type of self-organizing map, used to evolve useful samples according to the above mechanism artificially. The eigenvectors of the input correlation matrix are called the principal components, which are composed of the corresponding linear subspaces. In fact, we released a draft idea of an adaptive subspace self-organizing map in [31], and we extended this idea and made a comprehensive of the EASSOM algorithm by the presence of the structure and learning scheme in this section.

An invariant feature of the input vector \mathbf{x} represents the signal subspaces. A linear subspace L of dimensionality H is defined given the linearly independent basis vectors $\mathbf{b}_1, \dots, \mathbf{b}_H$, and the reconstructed signal is obtained as shown in Eq. (1); however, there exist infinitely many equivalents and non-unique combinations of the \mathbf{b}_h for the same L . In the parameter learning phase, this study utilizes a gradient descent (GD) algorithm to achieve updating. The detailed functions of each layer are described below.

A. EASSOM Structure

EASSOM presents a module structure, as in Figure 1. Three layers are included, layer 1 takes input data, layer 2 maps the input data to feature space(subspace), and layer 3 manages to reconstruct original data. Each node in layer 2 can be represented as a linear-subspace neural unit. Each node is a linearly independent basis vector. The output function of layer 3 is written as

$$\hat{\mathbf{x}} = \sum_{i=1}^H \mathbf{x} \mathbf{b}_i \mathbf{b}_i^T \quad (1)$$

where \mathbf{x} denotes input data, \mathbf{b}_i denotes the orthonormal form, and H denotes the number of hidden nodes.

Here, a set of equivalent orthonormal basis vectors for L can be computed by the familiar Gram-Schmidt process. The reconstructed signal relies on the orthonormal basis; in other words, the reconstructed signal $\hat{\mathbf{x}}$ that belongs to L is the

orthogonal projection of \mathbf{x} onto L .

We expect that the reconstructed signal is approximately similar to the original signal; thus, the criterion using the Euclidean distance as $\|\hat{\mathbf{x}}\| = \|\mathbf{x} - \hat{\mathbf{x}}\|$ is present to determine whether they are similar or even identical. Finally, a projection operator matrix P is defined as Eq. (2), and the following properties hold: $P^2 = P$ and $P^T = P$.

$$P = \sum_{i=1}^H \mathbf{b}_i \mathbf{b}_i^T \quad (2)$$

where $\hat{\mathbf{x}} = P\mathbf{x}$ and $\tilde{\mathbf{x}} = (I - P)\mathbf{x}$, in which I represent the identity matrix.

B. Learning Scheme

Because the learning mechanism of the SOM is inherited, an EASSOM also possesses the abilities of competitive learning for parameter learning, which are vital contributions to the effectiveness and robustness of the system. First, we would like to describe the procedure of competitive learning, as in Figure 2. The different modules are generated to compete on the input signal subspaces to find the minimum distance as the winner, which represents important information in that a given signal subspace that is best wins; The number of competing for the module is defined by the expression

$$\begin{aligned} N &= \text{round} \left(\frac{\# \text{ of majority class}}{\# \text{ of minority class}} \right) - 1 \\ &= \text{round}(\text{imbalance ratio}) - 1. \end{aligned} \quad (3)$$

where N denotes the number of competing modules.

Consequently, the updated weight vectors in each module follow the representative winner. As the modules in the neighborhood of the winner are adapted to represent the input better, the neighboring modules gradually approximate the winner of the inputs. The representative winner can be defined by the expression

$$\begin{aligned} c &= \text{argmin}_{n \in N} \left\{ \sum_{t \in S} \|\mathbf{x} - \mathbf{x}^n(t)\|^2 \right\} \\ &= \text{argmin}_{n \in N} \left\{ \sum_{t \in S} \|\widehat{\mathbf{x}}^n(t)\|^2 \right\} \end{aligned} \quad (4)$$

where S is denoted as the total number of input samples and c as the index of the winning module.

After obtaining the winning module via competitive learning, the free parameters of the other modules must be adjusted dependently by a factor in terms of the distance between their input subspace and the subspace of the winning module, to achieve the phase of learning effectively. Therefore, we define the objective as minimizing the error function. The error function is considered to be expressed by the two factors that correspond to the neighborhood factors, $g_c^n(t)$, as follows:

$$g_c^n(t) = \exp \left[-\frac{\|\mathbf{x}^c(t) - \widehat{\mathbf{x}}^n(t)\|^2}{2\sigma^2} \right] \quad (5)$$

where σ is a constant.

Cost function E is defined as the summation of projection error for all modules and data.

$$E = \sum_n \sum_{t \in S} g_c^n(t) \|\mathbf{x}^n(t)\|^2 \quad (6)$$

Consequently, this GD algorithm is performed for each piece of incoming data. By using the GD algorithm for the updated basis vectors of each module, we have

$$\mathbf{b}_i^n(t+1) = \mathbf{b}_i^n(t) - \eta \frac{\partial E}{\partial \mathbf{b}_i^n(t)} \quad (7)$$

where \mathbf{b}_i^n is the i^{th} basis vector of module n and the factor η is a learning rate, and the derivation is computed as

$$\frac{\partial E}{\partial \mathbf{b}_i^n(t)} = -2 \sum_{t \in S} g_c^n(t) \mathbf{x}(t) \mathbf{x}(t)^T \mathbf{b}_i^n(t) \quad (8)$$

Based on Eqs. (7) and (8), the basis vectors are updated as follows:

$$\mathbf{b}_i^n(t+1) = [I + \eta g_c^n(t) \mathbf{x}(t) \mathbf{x}(t)^T] \mathbf{b}_i^n(t) \quad (9)$$

In the case of the rotation operation, the learning rate η should be such that it guarantees a monotonically increasing function of $\|\widehat{\mathbf{x}}^n\|$ or a monotonically decreasing function of $\|\widehat{\mathbf{x}}^n\|$. For the monotonic correction, we must be proportional to $\mathbf{x}^T \mathbf{b}_i^n$, and thus, one of the simplest ways is to divide the learning rate η by the crisp value $\|\widehat{\mathbf{x}}^n\|/\|\mathbf{x}\|$. Let us denote the learning rate as λ ; then, Eq. (9) is rewritten as

$$\mathbf{b}_i^n(t+1) = \left[I + \bar{\lambda}^n(t) \frac{\mathbf{x}(t) \mathbf{x}(t)^T}{\|\widehat{\mathbf{x}}^n(t)\|/\|\mathbf{x}(t)\|} \right] \mathbf{b}_i^n(t) \quad (10)$$

where $\bar{\lambda}^n(t) = \eta g_c^n(t)$.

During the learning process, we set the magnitude of the small components of the basis vectors \mathbf{b}_i^n to zero to reduce those degrees of freedom; thus, **the** \mathbf{b}_i^n is forced to approximate the dominant frequency components by a dissipation effect $\bar{\mathbf{b}}_i^n$ which can be described by

$$\bar{\mathbf{b}}_i^n = \text{sgn}(\mathbf{b}_i^n) \cdot \max[\mathbf{0}, \text{abs}(\mathbf{b}_i^n) - \boldsymbol{\varepsilon}] \quad (11)$$

where $\boldsymbol{\varepsilon}$ is a small fraction of magnitude vector that can be modeled as the following equation:

$$\boldsymbol{\varepsilon} = \alpha \cdot \text{abs}[\mathbf{b}_i^n(t) - \mathbf{b}_i^n(t-1)] \quad (12)$$

where α is a small constant. Based on the dissipation effect, $\boldsymbol{\varepsilon}$ requires to be applied after the GD algorithm is performed and prior to normalization. To ensure basis vectors of all competing modules are orthonormal, the Gram-Schmidt process is applied.

To sum up, since the set of basis vectors associated with a module is required twice, once to compute Equation (1), to make an efficient network implementation, a quadratic neuron representing a module in the ASSOM has been expanded to an extended adaptive subspace self-organizing map (EASSOM) in Fig. 2 to have another layer of neurons so that a copy of the basis vectors is available for computation of Equation (1).

Finally, we address the learning steps of an EASSOM are as follows.

Once we receive each piece of training data, the procedure will be divided into the following steps:

Step 1: Generate the competing modules by Equ (3).

Step 2: Find the winning module by Equ. (4).

Step 3: Update the basis vectors of each module via a gradient descent algorithm by Equ. (10) and (11).

Step 4: Orthonormalize the basis vectors of each module via the Gram-Schmidt process.

IV. EXPERIMENTS AND RESULTS

To effectively display the performance from using different oversampling methods, we apply two fundamental classifiers, artificial neural networks (ANNs) and SVMs. ANNs and SVMs both play important roles in solving classification problems. In this study, we only these most common supervised learning classifiers, ANN and SVM, as we assume they are reliable to test the oversampling performance based on benchmark datasets and good at handling the EEG-based classification tasks.

The ANNs [32] possess the special characteristics of self-organization, adaptive learning capability, and robustness. ANNs are inspired by biological neural networks, and the structures of the ANNs are commonly composed of interconnected neurons (non-linearity mapping) that deliver information to each other. Multilayer Perception (MLP) is a popular class of ANNs, which is composed of several layers of neurons: an input layer, possibly one or several hidden layers, and an output layer. Each neuron's input is connected with the output of the previous layer's neurons, whereas the neurons of the output layer determine the class of the input feature vector.

The SVM [33] is a popular machine learning method for various learning tasks or classification applications. SVMs belong to the non-probabilistic model that classifies unknown data using hyper-planes. The SVM implicitly maps samples to a high-dimensional space through a kernel trick instead of increasing a non-linear operation. In specific, an SVM uses a discriminant hyperplane to identify classes, and the selected hyperplane is the one that maximizes the margins, i.e., the distance from the nearest training points. Maximizing the margins is known to increase the generalization capabilities. Thus, the goal of the SVM method is to find a hyper-plane by which can separate the data into two parts. To construct a hyperplane in SVM, it needs to choose a linear or non-linear kernel. The radial basis function (RBF) kernel, a popular non-linear kernel function, used in various kernelized learning algorithms, particularly in SVM classification.

A. Benchmark Data

Eight benchmark datasets from the UCI machine learning repository [34] and KEEL dataset [35] are employed to test the

Table 1. Information on the imbalanced data sets

Dataset Name	# of Total Examples	# of Attributes	Minority Class	Majority Class	# of Minority Examples	# of Majority Examples	Imbalanced Ratio
Abalone	731	7	Class of '18'	Class of '9'	42	689	16.40
Breast cancer	683	9	Class of 'malignant'	Class of 'benign'	239	444	1.86
E. coli	336	7	Class of 'im'	All other classes	77	259	3.36
Glass	214	9	Class of '5,6,7'	All other classes	51	163	3.20
Pima	768	8	Class of '1'	Class of '0'	268	500	1.87
Vehicle	846	18	Class of 'van'	All other classes	199	647	3.25
Yeast	1484	8	Class of 'ME3', 'ME2', 'EXC', 'VAC', 'POX', 'ERL'	All other classes	304	1180	3.88
Ozone	1848	72	Class of '1'	Class of '0'	57	1791	31.42

proposed method compared with other existing oversampling or synthetic data generation technologies. Four assessment metrics, including the recall, precision, G-mean, and F1-value, are considered to reveal the significant advantage of the proposed method. Finally, the results demonstrate that we must account for the oversampling techniques to avoid having the classification of the minority party dominated by the majority party. Specifically, the information contributions from the minority party are more important than those from the majority party.

B. Assessment Metric

Four assessment metrics, the recall, precision, G-mean, and F-value, are considered to determine the benefits of the EASSOM for imbalanced class distributions. Four metrics reply by counting the number of true positive (TP), true negative (TN), false positive (FP), and false negative (FN) samples. These metrics are shown in Eqs. (28) - (31).

$$Precision = \frac{TP}{TP+FP} \quad (28)$$

$$Recall = \frac{TP}{TP+FN} \quad (29)$$

$$G - mean = \sqrt{\frac{TP}{TP+FN} \times \frac{TN}{FP+TN}} \quad (30)$$

$$F1 - value = 2 \frac{Recall \times Precision}{Recall + Precision} \quad (31)$$

The function G-mean is to evaluate the overall performance of a classifier associated with the accuracies on both the positive and negative class samples. Unlike the G-mean, which concerns both classes, the F1-value measures the effectiveness of the classification in terms of a ratio of the weighted importance on either the recall or precision for a single class.

C. Evaluation Results

This section presents the performance of the EASSOM and compares it with other state-of-the-art methods. The proposed EASSOM in this paper has been successfully validated on eight

real-world imbalanced problems from the UCI machine learning repository and KEEL dataset repository, including Abalone, Breast cancer, E. coli, Glass, Pima, Vehicle, and Yeast. These sets are chosen such that they have different characteristics in terms of their samples, features, classes, and imbalanced ratios. Some of these datasets have samples of more than two classes. For simplicity, these datasets are transformed into a two-class problem in this study. Table 1 describes the relevant items that are associated with data attributes and properties. There exist highly imbalanced ratios in the presence of the problems that have two categories.

Extensive experiments with two well-known supervised learning methods, ANNs and SVMs, demonstrate the performance of each dataset on the classification task after employing different oversampling approaches. The proposed method is evaluated by the before-and-after test to show the improvement compared to the classifiers that were constructed based on primitive datasets, for which the datasets are not oversampled. After the before-and-after test, the EASSOM is further compared to existing state-of-the-art approaches, namely, SMOTE, ADASYN, ESPO, MWMOTE, SVM-light, and SVM-balanced, to show the improvement realized by the proposed method.

For each comparative model in the validation process, 70% of the data are randomly selected to build the training data set, whereas the remaining data serve as test data. To maintain the imbalanced ratio in each dataset, the selection of majority and minority samples are processed from the original dataset, respectively. Furthermore, the classification task was conducted 50 times to evaluate each comparative classifier to prevent bias in the initial state parameters during the supervised learning procedure. This overall process of validation is repeated 5 times; hence, the average of 250 runs is compared against other methods.

The validation results of ANNs and SVMs with different oversampling approaches on the eight datasets are shown in Table 2 and Table 3, respectively. The best performance is shown in boldface. The results of the ANN and SVM show that our proposed EASSOM outperforms than existing methods for the majority of the real-world problems.

Table 2. Average ANN performance comparison for different comparative methods

Dataset	Measure	Original	SMOTE	ADASYN	MWMOTE	ESPO	EASSOM
Abalone	Recall	0.401	0.765	0.511	0.683	0.634	0.622
	Precision	0.414	0.355	0.345	0.426	0.299	0.446
	F1 value	0.394	0.483	0.407	0.518	0.404	0.513
	G mean	0.606	0.832	0.687	0.797	0.753	0.766
Breast cancer	Recall	0.862	0.940	0.902	0.9494	0.969	0.958
	Precision	0.937	0.934	0.936	0.929	0.936	0.947
	F1 value	0.896	0.937	0.918	0.938	0.952	0.952
	G mean	0.913	0.952	0.933	0.954	0.966	0.964
E. coli	Recall	0.714	0.864	0.734	0.818	0.863	0.887
	Precision	0.645	0.664	0.655	0.716	0.608	0.681
	F1 value	0.674	0.746	0.689	0.761	0.710	0.766
	G mean	0.791	0.863	0.803	0.858	0.846	0.879
Glass	Recall	0.817	0.863	0.790	0.871	0.859	0.880
	Precision	0.800	0.842	0.857	0.843	0.889	0.836
	F1 value	0.800	0.849	0.817	0.850	0.867	0.852
	G mean	0.870	0.903	0.867	0.906	0.908	0.908
Pima	Recall	0.556	0.739	0.634	0.708	0.677	0.655
	Precision	0.604	0.596	0.551	0.603	0.568	0.626
	F1 value	0.577	0.657	0.589	0.649	0.617	0.637
	G mean	0.667	0.730	0.677	0.726	0.700	0.716
Vehicle	Recall	0.898	0.949	0.935	0.962	0.967	0.969
	Precision	0.904	0.907	0.899	0.920	0.849	0.884
	F1 value	0.900	0.926	0.917	0.940	0.903	0.924
	G mean	0.933	0.959	0.951	0.968	0.956	0.964
Yeast	Recall	0.674	0.806	0.782	0.809	0.775	0.758
	Precision	0.730	0.636	0.558	0.641	0.649	0.721
	F1 value	0.700	0.710	0.650	0.714	0.706	0.736
	G mean	0.793	0.842	0.809	0.845	0.831	0.835
Ozone	Recall	0.035	0.360	0.358	0.362	0.499	0.280
	Precision	0.089	0.173	0.172	0.172	0.139	0.252
	F1 value	0.047	0.228	0.228	0.228	0.214	0.256
	G mean	0.094	0.572	0.569	0.566	0.659	0.513
Average	Recall	0.620	0.786	0.706	0.770	0.780	0.751
	Precision	0.640	0.638	0.622	0.656	0.617	0.674
	F1 value	0.624	0.692	0.652	0.700	0.672	0.705
	G mean	0.708	0.832	0.787	0.828	0.827	0.818
Average Rank	Recall	1.13	4.50	2.25	4.63	4.38	4.13
	Precision	3.50	3.38	2.63	4.00	2.50	4.75
	F1 value	1.13	4.00	2.25	4.75	3.25	5.13
	G mean	1.13	4.63	2.13	4.63	4.00	4.38
Average Overall Rank		1.72	4.13	2.31	4.50	3.53	4.59

To show the improvement of the proposed EASSOM better, all of the comparative approaches are ranked based on the results of each assessment metric. Under each assessment metric, the method with the best performance is scored as the highest points (ANN: 6 and SVM: 8), and the worst is scored as 1 point. Consequently, we compute the average rank of four-assessment metrics across the eight datasets to quantify the relative performances. By further averaging these four-assessment metrics, an overall assessment matrix is integrated to evaluate the comparative approaches. The ANN and SVM with the best performance, which possesses the highest number of points, are shown in the last row of Table 2 and Table 3. The average overall rank of the EASSOM is 4.59 for the ANN and 5.66 for the SVM, which is higher than any of the other state-of-the-art approaches. These experimental results suggest that our proposed EASSOM model can yield a significant improvement in the performance of the imbalanced correction.

V. EEG EXPERIMENT

After presenting the results of these experiments, two practical problems of electroencephalography (EEG) classification related to oversampling implementation are

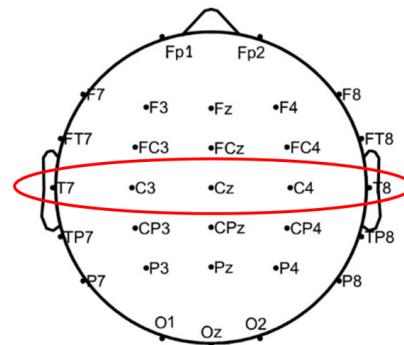


Figure 3. The measurement electrodes are placed across the sensorimotor area.

Table 3. Average SVM performance comparison for different comparative methods

Dataset	Measure	Original	SVM-Balanced	SVM-light	SMOTE	ADASYN	MWMOTE	ESPO	EASSOM
Abalone	Recall	0.202	0.769	0.143	0.567	0.422	0.447	0.655	0.477
	Precision	0.599	0.370	0.750	0.353	0.336	0.440	0.363	0.409
	F1 value	0.293	0.500	0.240	0.431	0.369	0.434	0.458	0.437
	G mean	0.418	0.840	0.327	0.716	0.626	0.652	0.773	0.674
Breast cancer	Recall	0.961	0.986	0.967	0.962	0.984	0.988	0.988	0.977
	Precision	0.945	0.932	0.947	0.932	0.931	0.935	0.928	0.946
	F1 value	0.952	0.958	0.957	0.947	0.956	0.961	0.957	0.961
	G mean	0.965	0.958	0.957	0.962	0.972	0.975	0.973	0.973
E. coli	Recall	0.761	0.773	0.779	0.776	0.773	0.843	0.925	0.863
	Precision	0.873	0.586	0.811	0.683	0.726	0.727	0.631	0.730
	F1 value	0.811	0.667	0.795	0.722	0.744	0.775	0.747	0.789
	G mean	0.857	0.673	0.795	0.829	0.837	0.869	0.878	0.882
Glass	Recall	0.789	0.667	0.882	0.876	0.890	0.885	0.862	0.871
	Precision	0.840	0.800	0.918	0.850	0.835	0.874	0.843	0.873
	F1 value	0.799	0.727	0.900	0.857	0.855	0.875	0.850	0.870
	G mean	0.860	0.730	0.900	0.91	0.914	0.919	0.904	0.913
Pima	Recall	0.536	0.685	0.571	0.613	0.560	0.643	0.735	0.694
	Precision	0.691	0.625	0.662	0.573	0.555	0.607	0.616	0.620
	F1 value	0.602	0.654	0.613	0.590	0.553	0.623	0.667	0.654
	G mean	0.681	0.654	0.615	0.679	0.648	0.706	0.740	0.731
Vehicle	Recall	0.952	0.983	1.000	0.960	0.935	0.962	0.991	0.956
	Precision	0.939	0.862	0.765	0.934	0.941	0.906	0.872	0.951
	F1 value	0.946	0.918	0.867	0.946	0.935	0.931	0.927	0.953
	G mean	0.966	0.968	0.875	0.969	0.957	0.964	0.973	0.970
Yeast	Recall	0.670	0.847	0.641	0.714	0.658	0.746	0.804	0.769
	Precision	0.810	0.537	0.809	0.678	0.591	0.646	0.624	0.670
	F1 value	0.733	0.658	0.716	0.695	0.621	0.690	0.702	0.715
	G mean	0.801	0.837	0.720	0.807	0.761	0.815	0.838	0.832
Ozone	Recall	0.197	0.181	0.287	0.285	0.199	0.311	0.327	0.184
	Precision	0.250	0.217	0.186	0.260	0.283	0.288	0.167	0.276
	F1 value	0.209	0.212	0.223	0.265	0.225	0.293	0.219	0.214
	G mean	0.421	0.398	0.516	0.516	0.434	0.540	0.542	0.413
Average	Recall	0.634	0.736	0.659	0.719	0.678	0.728	0.786	0.724
	Precision	0.743	0.616	0.731	0.658	0.650	0.678	0.631	0.684
	F1 value	0.668	0.662	0.664	0.682	0.657	0.698	0.691	0.699
	G mean	0.746	0.757	0.713	0.799	0.769	0.805	0.828	0.799
Average Rank	Recall	1.88	4.75	4.13	4.25	3.38	5.75	6.88	4.75
	Precision	6.25	2.63	6.00	3.88	3.25	5.25	2.63	6.00
	F1 value	4.00	3.50	4.63	3.88	3.25	5.50	4.75	6.00
	G mean	3.50	3.50	1.88	4.50	3.63	5.88	7.00	5.88
Average Overall Rank		3.91	3.59	4.16	4.13	3.38	5.59	5.31	5.66

addressed in this section. The collection of a considerable amount of valid EEG data typically has a high cost; however, the performance of the modeling is nonstationary if the data collection is insufficient.

With this motivation, this section applies the proposed EASSOM model to solve the problem mentioned above because it can automatically generate synthetic samples according to the distribution of the original data.

EEG data collection and analysis has attracted a substantial amount of attention for many years. A significant advantage of EEG over other extraction methodologies is that it provides convenient real-time measurements. Therefore, EEG signals are commonly used in real-world applications [36-38]. In the EEG-based brain-computer interface (BCI) design, well-recorded data are difficult to collect because most of the subjects are affected by interior and exterior disturbances.

These disturbances greatly reduce the quality of the collected data; therefore, the collection of substantial EEG data is always a challenge for constructing BCIs. In contrast, for recognition problems, if the data collection is insufficient, then the performance of the modeling is often nonstationary. The oversampling approach is intuitively considered to be an effective method to compensate for insufficient information by generating synthetic samples. In our study, the EEG signals collected from three experiments, motor imagery (MI) task, driving task, and migraine phases task, are used to validate the effect of the use of our proposed EASSOM in the classification purpose. All experiments were approved by the Institutional Review Board at Taipei Veterans General Hospital. Informed consent was obtained from all subjects before they joined the study.

Table 4. Classification performance of each channel in subject 1 to test the remaining subjects in the MI task.

Training subject	Test subject	w/o oversampling (Mean + SD %)	w oversampling (Mean + SD %)	IR	Training subject	Test subject	w/o oversampling (Mean + SD)	w oversampling (Mean + SD)	IR
Subject 1 (1 st channel)	Subject 2	75.0±15.6	82.5±11.7	7.5%	Subject 1 (3 rd channel)	Subject 2	37.5±11.0	51.9±11.0	14.4%
	Subject 3	65.0±14.2	73.8±6.5	8.8%		Subject 3	62.5±11.4	66.3±8.9	3.8%
	Subject 4	60.0±6.7	63.6±5.1	3.6%		Subject 4	48.8±9.7	58.8±8.9	10.0%
Subject 1 (2 nd channel)	Subject 2	55.0±15.3	70.6±14.1	15.6%	Subject 1 (4 th channel)	Subject 2	52.5±12.2	60.8±14.2	8.3%
	Subject 3	60.5±8.9	64.6±10.6	4.1%		Subject 3	46.3±11.9	59.4±14.2	13.1%
	Subject 4	51.8±10.5	63.8±14.4	12.0%		Subject 4	53.1±6.1	60.2±9.9	7.1%

A. Motor Imagery (MI) Task

1) Experiment and subjects

Four healthy young adults participated in the MI experiment in this study. For each subject, the EEG data were collected across the sensorimotor area, as shown in Figure 3. Each subject was instructed to sit on a standard chair and keep his/her hands placed on a table statically. During the MI task, the screen was kept blank for 2 seconds at the beginning of each trial. A cross mark was then displayed on the center of the screen for 2 seconds as an alarm prior to the left/right imagery event. Subsequently, a left/right arrow mark was randomly introduced on the screen for 10 seconds. During this 10 seconds imagery period, the participants were required to imagine the left/right-hand movement in accordance with the direction of the arrow that appears. After the end of the imagination, the inter-trial intervals of random imagery events were set to 7-10 seconds. The MI paradigm consisted of four sessions, in which each session consisted of 40 trials.

2) EEG signal processing

In this study, EEG was used to measure each participant's brain dynamics during the MI task. All of the EEG data were recorded using a portable 4-channel EEG recording device with dry spring-loaded sensors [39]. The EEG data were recorded at a sampling rate of 512 Hz by the hardware specifications. Then, down-sampling to 100 Hz was applied to reduce the computational complexity during the subsequent

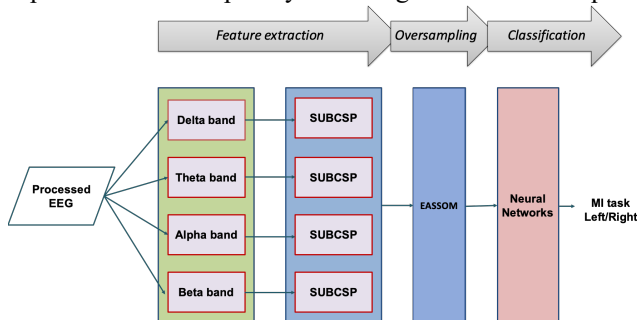


Figure 4. Scheme composed of the filter bank, SUBCSP, EASSOM, and NN classifier.

computational phase. The acquired EEG data were thereby processed and analyzed during the pre-processing stage for band-pass filtering, down-sampling, epoch extraction, and artificial removal. For each channel of interest associated with the cerebral cortex, the mean powers in the delta (1-3 Hz), theta (4-7 Hz), alpha (8-12 Hz) and beta (13-30 Hz) bands were collected for power spectrum analysis and feature extraction.

The main concept of using a common spatial pattern (CSP) [40] is to exploit a linear transformation to project the multi-channel EEG signals into low-dimensional spatial subspaces with a projection matrix, of which each row consists of weights for different channels. Significant channels were selected by searching the maximums of the spatial patterns in scalp mappings. Although the CSP is effective for manually finding the optimal band for each subject, it is also time-consuming, and the result is hardly repeated by other research groups.

Although it is effective to find a subject-specific frequency range for each subject manually, it is time-consuming, and the result is nonstationary. Here, we employ a filter bank to decompose the EEG signals into 4 sub-bands: delta, theta, alpha, and beta bands as inputs to the CSP. This method refers to the sub-band CSP (SUBCSP) [41], which has proven to achieve a similar result to that of finding proper bands manually for each subject. In previous studies [41, 42], it is difficult for CSP to consider both the accuracy and efficiency simultaneously, but SUBCSP can achieve this feature. Figure 4

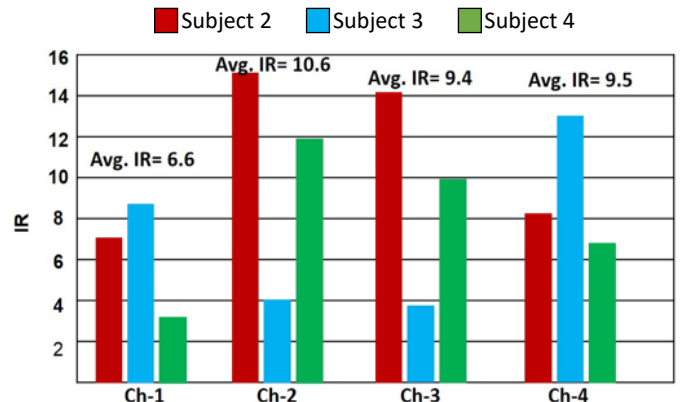


Figure 5. Improvement rate (IR) results.

Table 5 Fatigue state identification of driving task

EEG power & coherence	State [Accuracy (Mean + SD %)]	$Cluster_{Low\ Fatigue}$	$Cluster_{Medium\ Fatigue}$	$Cluster_{High\ Fatigue}$
w/o oversampling	<i>Low Fatigue</i>	74.8±1.3	8.1±1.4	16.9±2.8
	<i>Medium Fatigue</i>	40.7±2.2	24.4±5.7	34.9±2.9
	<i>High Fatigue</i>	31.2±2.4	23.8±1.0	45.0±2.2
w oversampling	<i>Low Fatigue</i>	78.7±4.3	10.2±3.4	11.2±2.8
	<i>Medium Fatigue</i>	37.1±9.2	46.4±7.2	16.6±4.9
	<i>High Fatigue</i>	20.7±1.8	9.7±2.0	69.6±3.2
IR %	Overall	3.9%	24%	24.6%

shows the comprehensive scheme regarding the filter bank, SUBCSP, EASSOM, and neural networks. Delta, theta, alpha, and beta bands are features for EASSOM to take the band features of minority class to generate synthetic data for balancing the MI dataset. To be specific, following the Figure 4 and Table 4, the input data for EASSOM are the band features of subject 1. Subjects 2-4 follow the EEG pre-processing procedure and feature extraction stage as Subject 1 to act as the testing set.

3) Evaluation results

To select the optimal channel used in the MI task, the channels in each subject were divided during the training phase in this study. For each subject, there were four input variables and 16 samples in each channel. The original (without oversampling) data are regarded as the baseline features for classification. To demonstrate the improvement of the use of the oversampling strategy, only one subject was employed as the representative of the sparse data for being oversampled. Subsequently, SVMs were trained using these oversampled data in the MI recognition task. In this study, we exploit the information from subject 1 to generate synthetic data as the training set, to test that of the remaining subjects. Please note we applied the same validation and classification process in the MI task as addressed in Section IV.

The system performance is shown in Table 4, in which we compare the results with and without the EASSOM approach. We present the style of the averaged classification accuracy with the standard deviation (SD) using ‘plus/minus small numbers’. For example, the value: 0.75 ± 0.15 represents 75% mean classification accuracy with 15.6% SD.

To better show the improvement from the use of EASSOM, we defined the improvement rate (IR) calculated by the difference of the classification performance in Table 4 between measurement with oversampling and without oversampling. Figure 5 illustrates the averaged IR of each channel of the overall 3 subjects (subjects 2, 3, and 4). Compared with the result without the oversampling approach, the average performance of each channel using the oversampling approach across three subjects boosts the results by 6.6%, 10.6%, 9.4%, and 9.5%. For example, in terms of 1st channel, and the averaged improvement rate is 6.6% by meaning the improvement rate from subject 1 to other 3 subjects (refer to Table 4, subject 2: $7.5\% = 82.5\% - 75.0\%$; subject 3: $8.8\% = 73.8\% - 65.0\%$; subject 4: $3.6\% = 63.6\% - 60.0\%$; the averaged improvement rate $6.6\% = (7.5\% + 8.8\% + 3.6\%)/3$). This

finding suggests that our proposed EASSOM model can offer sufficient information based on regulating the amount of sparse data while addressing EEG identification problems.

B. Driving Task

1) Experiment and subjects

In this study, 33 subjects with normal or corrected vision were recruited for the continuous attention driving experiment. Subjects were asked not to drink alcoholic or caffeinated beverages or participate in strenuous exercise the day before the experiment to ensure that their driving performance could be accurately assessed. Prior to the experiment, all subjects practiced driving in the simulator to be familiar with experimental procedures.

This task implemented an immersive driving environment [43], provided a simulated nighttime driving on a four-lane highway. Regarding the experimental paradigm, lane-departure events were randomly activated during the simulated driving to cause the car to drift away from the center of the cruising lane (deviation onset). The subjects were instructed to steer the car back (response onset) to the lane center (response offset) as soon as possible after becoming aware of the deviation. The lapse in time between the onset of deviation and response was defined as the reaction time (RT). The regulating attention determines the period of RTs, says ‘low fatigue’ corresponding to the short RT, and the ‘high fatigue’ corresponding to the long RT [44].

2) EEG signal processing

During the experiments, the EEG signals were recorded using Ag/AgCl electrodes that were attached to a 32-channel Quik-Cap (Compumedical NeuroScan). Thirty electrodes were arranged according to a modified international 10-20 system, and two reference electrodes were placed on both mastoid bones. The impedance of the electrodes was calibrated under $5k\Omega$, and the EEG signals recorded at a sampling rate of 500 Hz with 16-bit quantization. Before the data were analyzed, the raw EEG recordings were inspected manually to remove significant artifacts and noisy channels and pre-processed using a digital band-pass filter (1-30 Hz) to remove line noise and artifacts.

The EEG signal was estimated using 512-point fast Fourier Transformation (FFT). The step size was set to 1 sec (500 points). Each 512-points sub-window was then transformed to

Table 6. Classification performance of migraine phases task

EEG Coherence	Migraine Phases	Accuracy by EEG frequency band			
		Delta (Mean + SD %)	Theta (Mean + SD %)	Alpha (Mean + SD %)	Beta (Mean + SD %)
w/o oversampling	Overall	77.2 ± 10.1	92.2 ± 07.0	74.2 ± 10.2	62.3 ± 11.3
	Inter-ictal	90.3 ± 12.2	96.1 ± 06.2	86.3 ± 13.2	77.2 ± 17.6
	Pre-ictal	54.2 ± 23.0	85.4 ± 15.3	51.1 ± 23.0	35.2 ± 20.3
w oversampling	Overall	81.3 ± 12.2	93.4 ± 06.3	78.2 ± 11.5	66.1 ± 10.4
	Inter-ictal	87.1 ± 10.3	94.2 ± 07.0	84.4 ± 12.1	76.1 ± 15.1
	Pre-ictal	65.1 ± 15.4	88.4 ± 12.1	60.3 ± 18.1	44.5 ± 17.2
IR %	Overall	4.1%	1.2%	4%	3.8%

the frequency domain using 512-points FFT, and the mean value of all sub-windows in the frequency domain was calculated as the output of the FFT process. The EEG theta

power spectral has been identified to distinguish the cognition states: alertness and drowsiness [44]. Furthermore, the EEG coherence, a measure of the degree of similarity of the EEG recorded between pairs of channels, is also considered as the patterns to distinguish the states of low fatigue, medium fatigue, and high fatigue [44].

3) Evaluation results

A multidimensional feature vector consisting of EEG theta power and coherence of 30 channels is used to cluster the accuracy of (low, medium, and high) fatigue states by the Gaussian mixture model (GMM) [44]. As shown in Table 5, we compared the classification performance of clustering three fatigue states with and without the oversampling process. In specific, without the oversampling process, the classifications accuracies of low fatigue, medium fatigue, and high fatigue, are 74.8±1.3%, 24.4±5.7%, and 45.0±2.2%, respectively. However, if included with the oversampling process by our proposed EAASOM, the classification performance of low fatigue, medium fatigue, and high fatigue improved to 75.8±1.4%, 32.7±2.4%, and 55.9±1.0%, respectively.

C. Migraine Phases Task

1) Experiment and subjects

In this study, 43 patients with migraine without aura, as having low-frequency migraine (1-5 days per month) were invited to join this study [45]. Each patient kept a headache diary and completed a structured questionnaire on demographics, headache profile, medical history, and medication use. On EEG study days, patients' migraine phases were designated as inter-ictal or pre-ictal based on the patients' headache diaries. The pre-ictal phase was coded when patients were within 36 hours before a migraine attack on the day of EEG study, and the inter-ictal phase was coded for patients in a pain-free period between pre-ictal and after 36 hours of a migraine attack.

Experiments were performed in a quiet, dimly lightroom. During the first 2 minutes of the experiment, subjects were instructed to take several deep breaths while they adapted to the environment. Next, subjects were instructed to open their eyes

for 30 seconds and close their eyes for 30 seconds and to repeat this sequence for a total of three times. Meanwhile, EEG signals were digitized and recorded at a sampling rate of 256 Hz via a Nicolet One EEG System (Natus Ltd., USA). Eighteen EEG leads (Fp1, Fp2, F7, F3, Fz, F4, F8, T3, C3, Cz, C4, T4, T5, P3, P4, T6, O1, and O2) were placed according to the International 10–20 system. Fz was used as the reference channel.

2) EEG signal processing

During signal preprocessing, raw EEG signals were subjected to 1-Hz high-pass and 30-Hz low-pass finite impulse response filters. Filtered EEG data were inspected manually to remove artifacts and noisy channels (i.e., channels severely contaminated by eye movements, blinks, and muscle or heart activities). Eyes-open and eyes-closed resting-state signals of three blocks were extracted and concatenated for further analyses.

Similar to the previous task, the coherence index, an indicator of synchronization between paired channels, was used to establish the connectivity structure in each migraine phase [45]. This EEG coherence analysis was performed on pairs of EEG signals to determine the degree of synchronization between brain areas within particular frequency bands for migraine phases.

3) Evaluation results

In this study, we collected 30 inter-ictal patients and only 13 pre-ictal patients in total, because it is not easy to catch the short pre-ictal migraine phase. The feature dimensions of EEG coherence with 30 channels are 136. The original (without oversampling) data are regarded as the baseline features for classification. By EAASOM oversampling approach, we oversampled the number of pre-ictal EEG signals to 30, consistent with that in the inter-ictal phase. Please note we applied the same validation and classification process in the migraine phases task as addressed in Section IV. The classification performance of EEG coherence with and without oversampling approach in each cortical frequency band (delta, theta, alpha, and beta) are summarized in Table 6. Compared to the classification performance without oversampling, we note that oversampled EEG coherence using EAASOM can achieve the higher overall accuracy (from 77.2 ± 10.1 to 81.3 ± 12.2 in delta band, from 92.2 ± 07.0 to 93.4 ± 06.3 in theta band, from 74.2 ± 10.2 to 78.2 ± 11.5 in alpha band, and from 62.3 ± 11.3

to 66.1 ± 10.4 in beta band), as well as improve accuracy for the pre-ictal phase, based on a popular non-linear kernel RBF-SVM classifier.

VI. DISCUSSION AND CONCLUSION

In this paper, we proposed a promising and powerful method, EASSOM, which can effectively evolve useful samples using invariant features associated with rotation, translation, and scaling. To solve the imbalanced issues in the recognition problems and EEG applications, synthetic data are intuitively generated and inserted into the minority class, to reach the number of majority samples; therefore, classifiers trained via such an oversampling technology strategy can obtain superior performance compared with those that are trained with primitive imbalanced samples.

Considering a range of imbalance situations in the neuroscientific and neurological context, limited studies investigated the imbalance learning applying to EEG signals and BCI, and one recent study showed the possibility to generate artificial EEG signals with a generative adversarial network (GNN) [46]. However, we did not exploit the notion of GNN to generate time-series samples artificially, the EASSOM using the subspace concept shows competitive performance against conventional KNN-evolved approaches. Experimental benchmark and EEG results have demonstrated that the proposed EASSOM with the learning mechanism and the use of the subspace concept shows effective and robust among metrics.

In summary, the principal contributions of EASSOM are twofold. One is the learning ability, and the other is the use of the subspace concept. The learning procedure of an EASSOM is extended from SOM. As a result, the distinguished abilities of EASSOM still include competitive learning and adaptive learning strategies to effectively adjust all of the free parameters. The purpose of competitive learning is to obtain the best module (winner) means that the smallest distance compared to the rest of the modules, and then the updated weights, have been followed by the winner. Subsequently, the EASSOM learning procedure adjusts the subspace of the winning module to make the free weights of each module approach the raw signal in the input subspace.

REFERENCES

- [1] V. Chandola, A. Banerjee, and V. Kumar, "Anomaly detection: A survey," *ACM computing surveys (CSUR)*, vol. 41, no. 3, p. 15, 2009.
- [2] S. C. Tan, J. Watada, Z. Ibrahim, and M. Khalid, "Evolutionary fuzzy ARTMAP neural networks for classification of semiconductor defects," *IEEE transactions on neural networks and learning systems*, vol. 26, no. 5, pp. 933-950, 2015.
- [3] Q. Kang, X. Chen, S. Li, and M. Zhou, "A noise-filtered under-sampling scheme for imbalanced classification," *IEEE transactions on cybernetics*, vol. 47, no. 12, pp. 4263-4274, 2017.
- [4] P. Lim, C. K. Goh, and K. C. Tan, "Evolutionary cluster-based synthetic oversampling ensemble (eco-ensemble) for imbalance learning," *IEEE transactions on cybernetics*, vol. 47, no. 9, pp. 2850-2861, 2017.
- [5] H. He and E. A. Garcia, "Learning from imbalanced data," *IEEE Transactions on Knowledge & Data Engineering*, no. 9, pp. 1263-1284, 2008.
- [6] R. Batuwita and V. Palade, "FSVM-CIL: fuzzy support vector machines for class imbalance learning," *IEEE Transactions on Fuzzy Systems*, vol. 18, no. 3, pp. 558-571, 2010.
- [7] Z.-H. Zhou and X.-Y. Liu, "Training cost-sensitive neural networks with methods addressing the class imbalance problem," *IEEE Transactions on Knowledge and Data Engineering*, vol. 18, no. 1, pp. 63-77, 2006.
- [8] S.-J. Yen and Y.-S. Lee, "Cluster-based under-sampling approaches for imbalanced data distributions," *Expert Systems with Applications*, vol. 36, no. 3, pp. 5718-5727, 2009.
- [9] A. Manukyan and E. Ceyhan, "Classification of imbalanced data with a geometric digraph family," *The Journal of Machine Learning Research*, vol. 17, no. 1, pp. 6504-6543, 2016.
- [10] N. V. Chawla, K. W. Bowyer, L. O. Hall, and W. P. Kegelmeyer, "SMOTE: synthetic minority over-sampling technique," *Journal of artificial intelligence research*, vol. 16, pp. 321-357, 2002.
- [11] H. Han, W.-Y. Wang, and B.-H. Mao, "Borderline-SMOTE: a new over-sampling method in imbalanced data sets learning," in *International Conference on Intelligent Computing*, 2005: Springer, pp. 878-887.
- [12] N. V. Chawla, A. Lazarevic, L. O. Hall, and K. W. Bowyer, "SMOTEBoost: Improving prediction of the minority class in boosting," in *European conference on principles of data mining and knowledge discovery*, 2003: Springer, pp. 107-119.
- [13] S. Barua, M. M. Islam, X. Yao, and K. Murase, "MWMOTE--majority weighted minority oversampling technique for imbalanced data set learning," *IEEE Transactions on Knowledge and Data Engineering*, vol. 26, no. 2, pp. 405-425, 2014.
- [14] H. He, Y. Bai, E. A. Garcia, and S. Li, "ADASYN: Adaptive synthetic sampling approach for imbalanced learning," in *Neural Networks, 2008. IJCNN 2008. (IEEE World Congress on Computational Intelligence). IEEE International Joint Conference on*, 2008: IEEE, pp. 1322-1328.
- [15] H. Cao, S.-K. Ng, X.-L. Li, and Y.-K. Woon, "Integrated oversampling for imbalanced time series classification," *IEEE Transactions on Knowledge and Data Engineering*, p. 1, 2013.
- [16] C.-T. Lin *et al.*, "Minority Oversampling in Kernel Adaptive Subspaces for Class Imbalanced Datasets," *IEEE Transactions on Knowledge & Data Engineering*, no. 1, pp. 1-1, 2018.
- [17] T. Kohonen, "Emergence of invariant-feature detectors in the adaptive-subspace self-organizing map," *Biological cybernetics*, vol. 75, no. 4, pp. 281-291, 1996.
- [18] T. Kohonen, S. Kaski, H. Lappalainen, and J. Salj arvi, "The adaptive-subspace self-organizing map (ASSOM)," in *International Workshop on Self-Organizing Maps (WSOM'97), Helsinki, 1997*, pp. 191-196.
- [19] Y. Zhang, C. S. Nam, G. Zhou, J. Jin, X. Wang, and A. Cichocki, "Temporally constrained sparse group spatial patterns for motor imagery BCI," *IEEE transactions on cybernetics*, no. 99, pp. 1-11, 2018.
- [20] D. Iacoviello, A. Petracca, M. Spezialetti, and G. Placidi, "A classification algorithm for electroencephalography signals by self-induced emotional stimuli," *IEEE transactions on cybernetics*, vol. 46, no. 12, pp. 3171-3180, 2016.
- [21] Z. Cao, K.-L. Lai, C.-T. Lin, C.-H. Chuang, C.-C. Chou, and S.-J. Wang, "Exploring resting-state EEG complexity before migraine attacks," *Cephalalgia*, vol. 38, no. 7, pp. 1296-1306, 2018.
- [22] Z. Cao, C.-T. Lin, W. Ding, M.-H. Chen, C.-T. Li, and T.-P. Su, "Identifying Ketamine Responses in Treatment-Resistant Depression Using a Wearable Forehead EEG," *IEEE Transactions on Biomedical Engineering*, 2018.
- [23] C.-T. Lin *et al.*, "Forehead EEG in support of future feasible personal healthcare solutions: Sleep management, headache prevention, and depression treatment," *IEEE Access*, vol. 5, pp. 10612-10621, 2017.
- [24] C. M. Bishop, *Pattern recognition and machine learning*. Springer Science+ Business Media, 2006.
- [25] G. Lema tre, F. Nogueira, and C. K. Aridas, "Imbalanced-learn: A python toolbox to tackle the curse of imbalanced datasets in machine learning," *The Journal of Machine Learning Research*, vol. 18, no. 1, pp. 559-563, 2017.
- [26] P. J. Lisboa, H. Wong, P. Harris, and R. Swindell, "A Bayesian neural network approach for modelling censored data with an application to prognosis after surgery for breast cancer," *Artificial intelligence in medicine*, vol. 28, no. 1, pp. 1-25, 2003.

- [27] P. J. Lisboa *et al.*, "Partial logistic artificial neural network for competing risks regularized with automatic relevance determination," *IEEE transactions on neural networks*, vol. 20, no. 9, pp. 1403-1416, 2009.
- [28] A. Pourhabib, B. K. Mallick, and Y. Ding, "Absent data generating classifier for imbalanced class sizes," *The Journal of Machine Learning Research*, vol. 16, no. 1, pp. 2695-2724, 2015.
- [29] T. Joachims, "A support vector method for multivariate performance measures," in *Proceedings of the 22nd international conference on Machine learning*, 2005: ACM, pp. 377-384.
- [30] C.-C. Chang and C.-J. Lin, "LIBSVM: a library for support vector machines," *ACM transactions on intelligent systems and technology (TIST)*, vol. 2, no. 3, p. 27, 2011.
- [31] Y.-T. Liu, N. R. Pal, S.-L. Wu, T.-Y. Hsieh, and C.-T. Lin, "Adaptive subspace sampling for class imbalance processing," in *Fuzzy Theory and Its Applications (iFuzzy), 2016 International Conference on*, 2016: IEEE, pp. 1-5.
- [32] A. K. Jain, J. Mao, and K. M. Mohiuddin, "Artificial neural networks: A tutorial," *Computer*, vol. 29, no. 3, pp. 31-44, 1996.
- [33] Y. Liu and Y. F. Zheng, "Soft SVM and its application in video-object extraction," *IEEE Transactions on Signal Processing*, vol. 55, no. 7, pp. 3272-3282, 2007.
- [34] M. Lichman, "UCI machine learning repository," ed: Irvine, CA, 2013.
- [35] J. Alcalá-Fdez *et al.*, "Keel data-mining software tool: data set repository, integration of algorithms and experimental analysis framework," *Journal of Multiple-Valued Logic & Soft Computing*, vol. 17, 2011.
- [36] T. Chouhan, N. Robinson, A. Vinod, K. K. Ang, and C. Guan, "Wavlet phase-locking based binary classification of hand movement directions from EEG," *Journal of neural engineering*, vol. 15, no. 6, p. 066008, 2018.
- [37] L. Bi, H. Wang, T. Teng, and C. Guan, "A Novel Method of Emergency Situation Detection for a Brain-controlled Vehicle by Combining EEG Signals with Surrounding Information," *IEEE Transactions on Neural Systems and Rehabilitation Engineering*, 2018.
- [38] J. Meng, T. Streitz, N. Gulachek, D. Suma, and B. He, "3-dimensional Brain-computer Interface Control through Simultaneous Overt Spatial Attentional and Motor Imagery Tasks," *IEEE Transactions on Biomedical Engineering*, 2018.
- [39] L.-D. Liao *et al.*, "A Novel 16-Channel Wireless System for Electroencephalography Measurements With Dry Spring-Loaded Sensors," *IEEE Trans. Instrumentation and Measurement*, vol. 63, no. 6, pp. 1545-1555, 2014.
- [40] Y. Wang, S. Gao, and X. Gao, "Common spatial pattern method for channel selection in motor imagery based brain-computer interface," in *Engineering in medicine and biology society, 2005. IEEE-EMBS 2005. 27th Annual international conference of the*, 2006: IEEE, pp. 5392-5395.
- [41] Q. Novi, C. Guan, T. H. Dat, and P. Xue, "Sub-band common spatial pattern (SBCSP) for brain-computer interface," in *Neural Engineering, 2007. CNE'07. 3rd International IEEE/EMBS Conference on*, 2007: IEEE, pp. 204-207.
- [42] K. K. Ang, Z. Y. Chin, H. Zhang, and C. Guan, "Filter bank common spatial pattern (FBCSP) in brain-computer interface," in *Neural Networks, 2008. IJCNN 2008.(IEEE World Congress on Computational Intelligence). IEEE International Joint Conference on*, 2008: IEEE, pp. 2390-2397.
- [43] Z. Cao, C.-H. Chuang, J.-K. King, and C.-T. Lin, "Multi-channel EEG recordings during a sustained-attention driving task," *Scientific Data*, vol. 6, 2019.
- [44] C.-H. Chuang *et al.*, "Dynamically Weighted Ensemble-based Prediction System for Adaptively Modeling Driver Reaction Time," *arXiv preprint arXiv:1809.06675*, 2018.
- [45] Z. Cao *et al.*, "Resting-state EEG power and coherence vary between migraine phases," *The journal of headache and pain*, vol. 17, no. 1, p. 102, 2016.
- [46] K. G. Hartmann, R. T. Schirrmester, and T. Ball, "EEG-GAN: Generative adversarial networks for electroencephalographic (EEG) brain signals," *arXiv preprint arXiv:1806.01875*, 2018.